CHALMERS
UNIVERSITY OF TECHNOLOGY

Deep learning models for improved accuracy of a multiphase flowmeter

Measurement 206 (2023) 112254

Contents lists available at ScienceDirect

Measurement

journal homepage: www.elsevier.com/locate/measurement

Deep learning models for improved accuracy of a multiphase flowmeter

Mohammadreza Manami [a], Sadegh Seddighi [a,b,*], Ramis Örlü [c,*]

[a] Department of Mechanical Engineering, K.N. Toosi University of Technology, Tehran, Iran
[b] Division of Energy Technology, Chalmers University of Technology, Gothenburg, Sweden
[c] KTH Engineering Mechanics, SE-100 44 Stockholm, Sweden

ARTICLE INFO

Keywords:
Flow metering
Multiphase flow
Fluid mechanics
Deep learning

ABSTRACT

Measurement of oil and gas two-phase flow with variable flow regimes relies to a large extent on flow patterns and their transitions. Using multiphase flowmeters in flows with high gas volume fractions is therefore usually associated with large uncertainties. This work presents a dynamic neural network method to measure the flow rate using a nonlinear autoregressive network with exogenous inputs (NARX). Total temperature and total pressure are used as network inputs and the obtained results are compared with a multilayer perceptron (MLP). Comparison between modeling results and the experimental data shows that the NARX network can predict oil and gas flow with variable flow regimes with less error compared to the MLP model, e.g. an absolute average percentage deviation (AAPD) of 0.68% instead of 1.02%. The present work can hence be seen as a proof-of-concept study that should motivate further applications of deep learning models to facilitate enhanced accuracy in flow metering.

1. Introduction

Multiphase flow is important for many real-life applications such as oil and gas transport, chemical, mining, food industries [1], environmental [2,3], and pharmaceutical [4], as well as biomedical applications such as airflow in humans tracheobronchial airways [5,6]. In the oil and gas industry, multiphase flow metering is essential for well testing, field allocation, and production optimization [7].

Different methods are used for the measurement of multiphase flow [8,9], including differential pressure [10,11], V-cone [12,13], correlation-based [14], vortex shedding [15], positive displacement [16], and Coriolis-based [16]. Generally, a combination of sensors is required to determine shares of each phase in a multiphase flow. The sensors required for measuring the share of each phase in a multiphase flow include gamma-ray [17–19], capacitance and conductance [20], microwave [21], and near-infrared probes [8,9]. One of the emerging technologies for measuring multiphase flow rates is soft computing and virtual metering [22,23]. However, knowledge of the flow regime of multiphase flows is key in the accuracy of multiphase flow metering. In industrial multiphase flow meters, the uncertainty of the measurements increases in high gas volume fractions, and some commercial flow meters have a certain range of operation for measuring gas volume fractions [9].

Flow pattern maps are used as a tool for estimating the range of different flow patterns by changing the flow rate of gas and liquid in specific conditions and interpreting the variations. The flow patterns and their transitions are defined qualitatively from visual observations. Therefore, mapping of transitions between different flow patterns may vary between various experimental approaches and methods, thereby making it very challenging to deduce any general analytical description. In addition, the flow patterns transition is gradually occurring and depends on various parameters like fluid properties, pipe diameter as well as orientation [24–27]. Therefore, it is very hard to prepare a general flow pattern map that can accurately estimate a wide range of different two-phase flow patterns [28]. Flow patterns in the horizontal tube are classified into the annular flow, bubbly flow, stratified flow, slug flow, and plug flow [29]. In annular flows, a high gas flow rate causes a liquid layer to form along the pipe wall, similar to vertical flows, with the significant difference that the liquid film at the bottom of the pipe is much thicker than the top layer. Gas velocity and gravity affect the thickness of the liquid film. The liquid film around the tube may or may not be continuous. The liquid film may be wavy and the droplets usually disperse into the gas. Investigation of different multiphase flow patterns and their impact on the measurement accuracy, especially in the annular regime that has a high gas volume fraction, can be important for the development of soft computing methods.

* Corresponding authors at: Department of Mechanical Engineering, K.N. Toosi University of Technology, Tehran, Iran (S. Seddighi).
E-mail addresses: sadeghsk@kth.se (S. Seddighi), orlu@kth.se (R. Örlü).

https://doi.org/10.1016/j.measurement.2022.112254
Received 1 June 2022; Received in revised form 31 October 2022; Accepted 20 November 2022
Available online 25 November 2022

Soft computing techniques that are widely used in multiphase flow meters (MPFMs) include machine learning (e.g. deep learning, neural networks, support vector machine), fuzzy logic, and evolutionary computing (e.g. genetic algorithms, evolutionary programming, etc.), [23]. Different investigations have been made on measuring individual phases in multiphase flow rates across the pipeline using soft computing techniques [30–41]. Soft computing input parameters can be mainly divided into five groups: 1) gamma-ray densitometer [18], 2) electrical signals [42], 3) ultrasonic data [43], 4) pressure signals [44] 5) fluid properties (such as temperature, density, and viscosity).

Machine learning methods have been used in several investigations of multiphase flow measurements [39] and flow over a choke [41]. Besides, extreme learning machine (ELM) is used for various types of problems (e.g. regression, classification, clustering, etc.) and it has advantages such as single hidden layer, reduced training parameters compared to typical models and improved generalization ability and convergence speed [45]. Deep learning (DL) models however provide powerful approximation and generalization abilities for non-linear data and give time series prediction solutions [46]. One of the novel methods for forecasting multiphase flow rate using deep learning was proposed by Alakeely et. al [40] by applying Gilbert correlation to DL algorithms for solving problem of liquid flow prediction wellhead surface measurements.

Artificial neural network (ANN) architecture was one of the methods used to estimate the volume fraction in an annular multiphase regime including oil, water, and gas by means gamma-ray detector [47]. The volume fractions of gas–oil–water in the three-phase annular flow were predicted using an adaptive neuro-fuzzy inference system (ANFIS) and an optimization algorithm for the training process by Karami et al. [18].

It can be seen in the literature that the measurement of multiphase flow with variable flow regimes using machine learning methods has been less studied. Also, in previous studies, the accuracy of multilayer perceptron has been observed more than other machine learning methods [48].

The aim of this work is to assess a dynamic neural network to measure the two-phase flow rate of oil and gas with variable flow regimes. In this research, a nonlinear autoregressive network with exogenous inputs (NARX), which is a recurrent dynamic network, has been investigated to increase the measurement accuracy. Total temperature and total pressure are used as network inputs to predict oil and gas flow rates separately. The obtained results are compared with multilayer perceptron. The present work can hence be seen as a proof-of-concept study for improving multiphase flow metering in flows with high gas volume fractions which are usually associated with high uncertainty.

2. Measurement

A differential pressure (Venturi) multiphase flow meter system was used to measure the multiphase flow rate. The multiphase flowmeter system can measure the flow rates of oil, water, and gas continuously without separating the fluids. This flowmeter is based on differential pressure (Venturi) and operates on the principle that any obstruction in the pipeline causes a pressure drop in the flow path. For the vertical Venturi, the volumetric flow rate can be calculated using the following equation [9]:

$$Q = C_d A_t \, \Upsilon \sqrt{\frac{2(\Delta P + \rho g \Delta z)}{\rho\left(1-\beta^4\right)}} \tag{1}$$

where $\triangle$P is the pressure difference, β is the ratio between diameter of the throat and the tube, A_t is the area of the throat, g is gravity and ρ is the density of the fluid, C_d is discharge coefficient, and is defined as the ratio of the actual discharge to the ideal discharge [49], ϒ is the expansion coefficient which considers the difference between the discharge coefficient for compressible (C_{dc}) and incompressible (C_{di}) flows. The expansion coefficient is defined as [50]:

$$\Upsilon = \frac{C_{dc}}{C_{di}} \tag{2}$$

Where ϒ is determined empirically and the relationships are presented in the American Gas Association (AGA) and International Organization for Standardization (ISO) [51,52]. For incompressible flow is ϒ = 1. The determination of the fluid fractions needs the measurement of two fluid properties. The flowmeter utilized in this work uses capacitance and conductance sensors to measure the volume fraction of each phase. Flowmeter's performance is based on the different capacities and conductivities of the phases in the multiphase flow (oil, gas, and water). The sensor consists of an electrode ring that can act as a capacitive and conductive device for measuring phase fractions (Fig. 1).

Capacity, C_m, and resistance, R_m, of the multiphase fluid can be determined using the following equations [8]:

$$C_e = \frac{\left[1+\omega^2 R_m^2 C_m\left(C_m + C_p\right)\right] C_p}{1+\omega^2 R_m^2 \left(C_{m+} C_p\right)^2} \tag{3}$$

$$R_e = \frac{1+\omega^2 R_m^2 \left(C_m + C_p\right)^2}{\omega^2 R_m C_p^2} \tag{4}$$

where ω is the excitation frequency of the electrodes, and C_p is the capacity of the pipeline wall.

3. Data description

A multiphase flow measurement test is performed to ensure proper well performance after workover (repair of an existing well). In this work, the dataset was measured in real-time using the commercial MPFM device. The studied well is located in oil field in southwestern Iran, and it is the completion string with a diameter of 4–1/2 in 5 inches. The dataset contains 4112 samples, and each sample includes temperature, pressure, oil flow rate, and gas flow rate of the multiphase flow. The data points are recorded at 1-minute intervals. Fig. 2 shows variations in oil flow rate, gas flow rate, pressure, and temperature over time measured in the experiments. The choke size was decreased from 32/64 to 16/64 in. during the measurement test. Due to unsteady and variable well conditions, temperature and pressure have large variations.

The statistical description of the dataset is presented in Table 1, which includes the mean, standard deviation, minimum, first quartile, median or second quartile, third quartile, and maximum values.

The pairs plot is a method to identify trends for further analysis. The pairs plot is used to show the pairwise relationships in the dataset, and diagonal plots show the distribution of each variable [53]. This plot often gives valuable insights. For example, in Fig. 3 shows how the oil and gas flows have been increasing with the increased pressure. Also, the relationship between flow rates and pressure is stronger than temperature. The nonlinear relationship between the variables is noticeable.

Fig. 4 shows the correlation coefficient for each pair of variables in the dataset. Comparison of the input variables correlation with flow

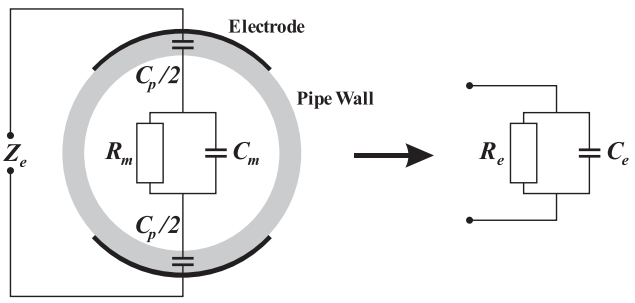

Fig. 1. Principle of impedance measurement in MPFM.

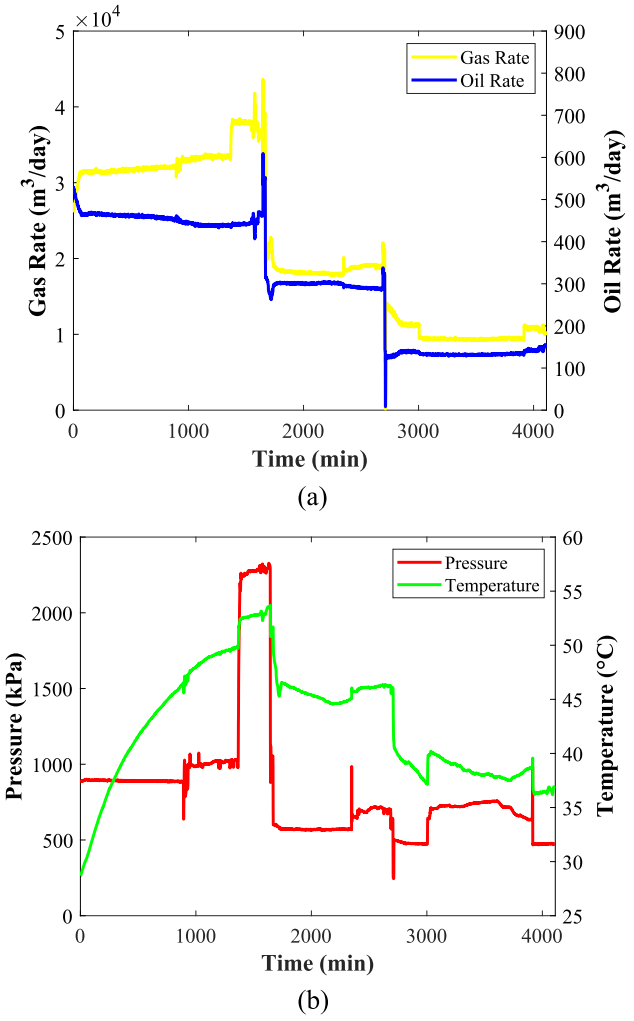

Fig. 2. Oil flow rate and gas flow rate (a), pressure and temperature (b).

Table 1
Statistical description of the dataset. The dataset contains 4112 samples. Note that the number of decimal places does not indicate accuracy of data.

	Pressure	Temperature	Oil Rate	Gas Rate
	(kPa)	(°C)	(m^3/day)	(m^3/day)
mean	836.78	42.69	306.58	21618.90
std	415.02	5.37	139.23	10211.67
min	244.82	27.93	8.34	141.58
25%	572.72	38.22	136.20	10873.67
50%	725.36	43.72	300.89	18689.12
75%	892.69	46.17	447.79	31856.45
max	2327.29	53.69	609.23	43636.26

rates indicates that pressure and temperature present a high correlation with flow rates. Based on Bernoulli's equation increased pressure causes an increased flow rate. Also, in an ideal gas, the temperature is directly dependent on the kinetic energy of the molecules. This evaluation of the inputs parameters' correlation degree with flow rates can assist in the proper selection of features to enhance performance of the models. Considering the nonlinear relationship between the features and the flow rates, a flow estimation method based on artificial neural networks is proposed in Section 4.

4. Methodology

Neural network modeling can be divided into two groups: the first one is the static architecture that uses feed-forward connections to calculate the output from input directly. The second one is dynamic architecture in which the output depends not only on its current inputs but also on the previous behavior of the network. In this study, static (MLP) and dynamic (NARX) neural networks have been used to model the multiphase flow meter with variable flow regimes. The structure of static and dynamic networks is explained below.

4.1. Multilayer perceptron (MLP)

In static architecture, multilayer perceptron (MLP) is the most widely utilized structure [54,55], which is used for a wide range of different problems. In an artificial neural network, there are multilevel sets of neurons. Neurons (which are called perceptrons in this context) of the input layer receive the data. The corresponding mapping for a two-layer MLP with d input nodes (index i), n hidden neurons (index j), and an output neuron can be written as below [23]:

$$y = f_o\left[\sum_{j=1}^{n} w_j \bullet f_h\left(\sum_{i=1}^{d} w_{ij}x_i + b_{hj}\right) + b_o\right] \tag{5}$$

Where x_i and y are the model inputs and outputs, respectively. Here, w_{ij} are the weights for connections (n × d) between the input nodes and the hidden neurons, the w_j are the weights for connections between the hidden and output neurons, and the b_h and b_o are bias terms for the hidden and output neurons, respectively. The activation function is denoted by f which is the source of nonlinearity in neural network. The linear activation function is only used at the output layer of neural network. Fig. 5 shows the architecture of the two-layer perceptron in the MLP model with d input and one output.

4.2. Nonlinear auto-regressive model with exogenous inputs (NARX)

NARX network was used for time series modeling in various fields recently [56–58]. NARX model is a recurrent dynamic neural network that relates the current value of a time series to the two following values:

- past values of the same series.
- current and past values of the exogenous series.

Exogenous series are the specified external series that affect the target series. The NARX mathematical model, which also expresses its dynamic behavior, is defined as [59–61]:

$$y(k+1) = F[y(k), y(k-1), \cdots y(k-d_o); X(k+1), X(k)\cdots X(k-d_i)] \tag{6}$$

Where y(k) is the previous value of the target and X(k) is the exogenous series. Here, d_i and d_o are the input and output lags, respectively. Using the appropriate activation functions f and biases b, the output result can be expressed as Eq. (7). Fig. 6 shows the structure of the NARX network [62].

$$y(k+1) = f_o\left[\sum_{j=1}^{n} w_{oj} \bullet f_h\left(\sum_{i=0}^{d_i} w_{xi}X(k+1-i) + \sum_{i=0}^{d_o} w_{yi}y(k - i) + b_{hj}\right) + b_o\right] \tag{7}$$

In the NARX model outputs relate to past values of the same series, for example in this case predicted values of oil and gas rates relate to temperature, pressure, and past values of oil and gas rates. But in the MLP model outputs just relate to the inputs (e.g. temperature and pressure).

Owing to the unsteady nature of oil and gas extraction from wells, such multiphase flows can be considered as time series [63]. NARX models are commonly used in time-series modeling which can be also suitable for oil and gas multiphase flow machine learning models.

Table 2 shows the list of hyperparameters after tuning. Hyperparameters include the number of layers, number of neurons in each

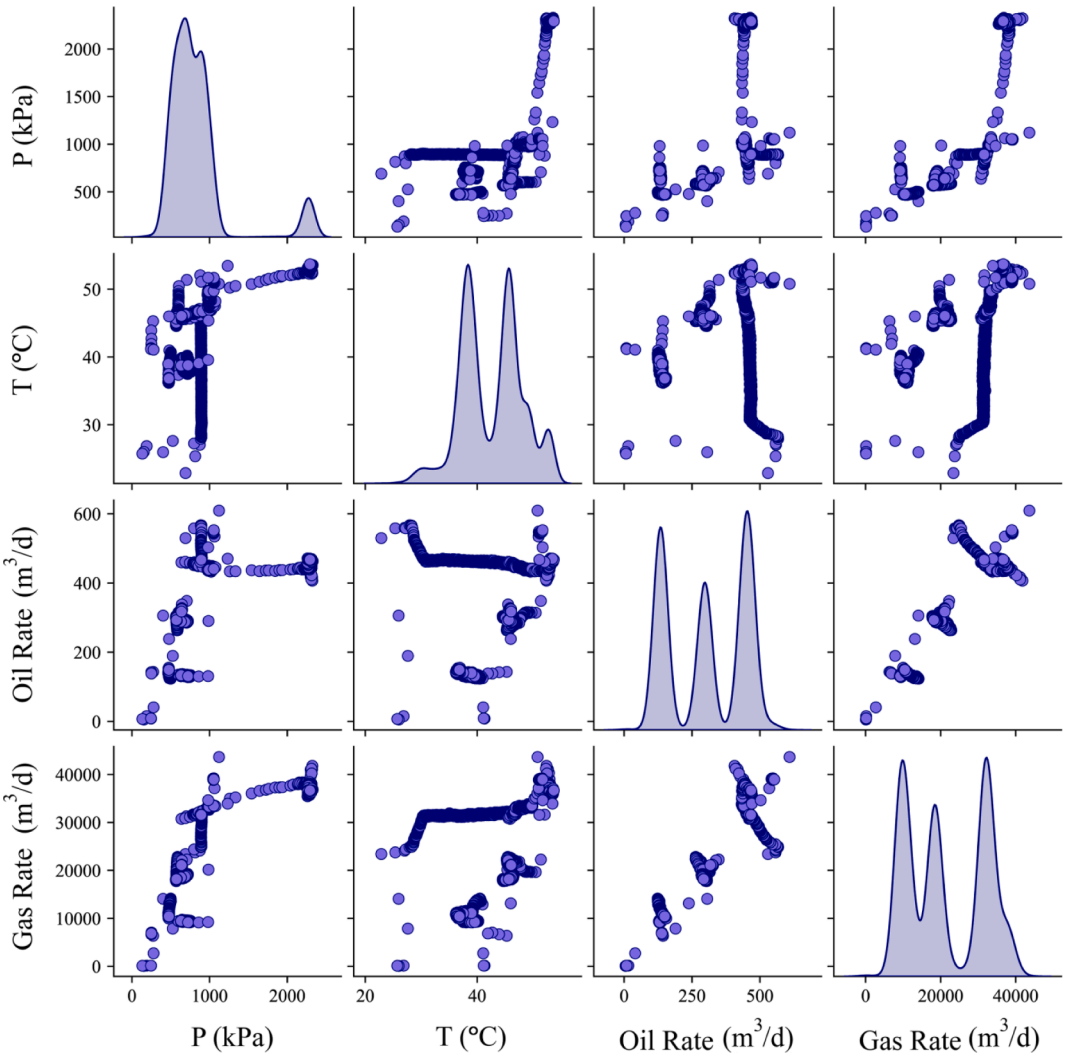

Fig. 3. Pairwise correlation in the dataset.

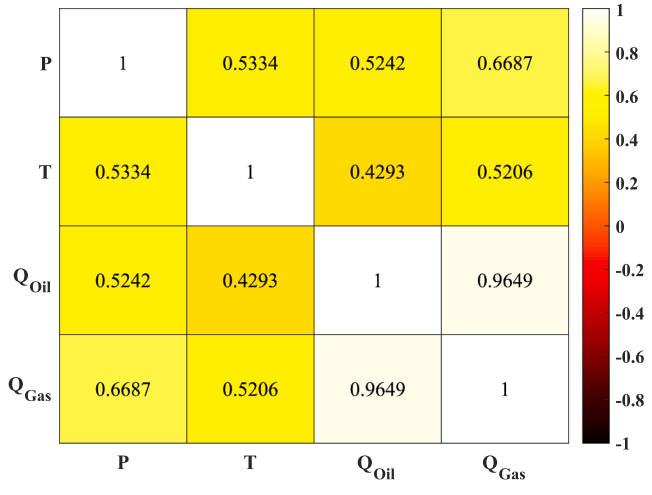

Fig. 4. Heatmap plot of Pearson's correlation coefficient.

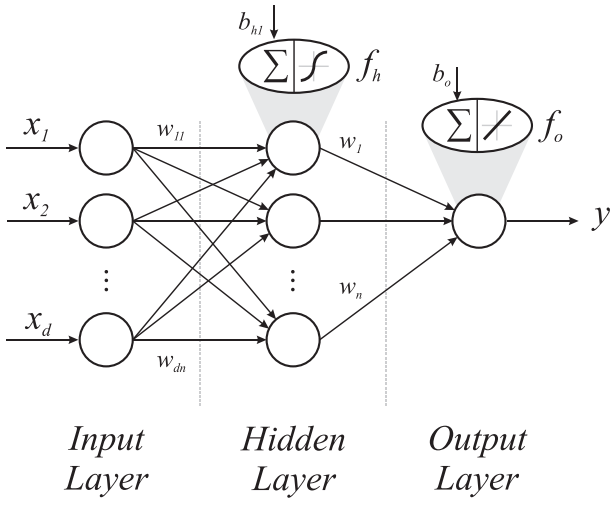

Fig. 5. Architecture of two-layer perceptron.

layer, activation function, number of epochs, and training algorithm for both MLP and NARX networks. Additionally, the number of delays for the NARX network is mentioned. For tuning of hyperparameters, a number of neurons and layers was obtained manually by gride search in the domain of 5 to 60 neurons for each layer. For selecting a number of epochs early stopping method was used to prevent from overfitting.

To compare the performance of MLP and NARX models, each network is trained using the dataset. The training and test sets selection

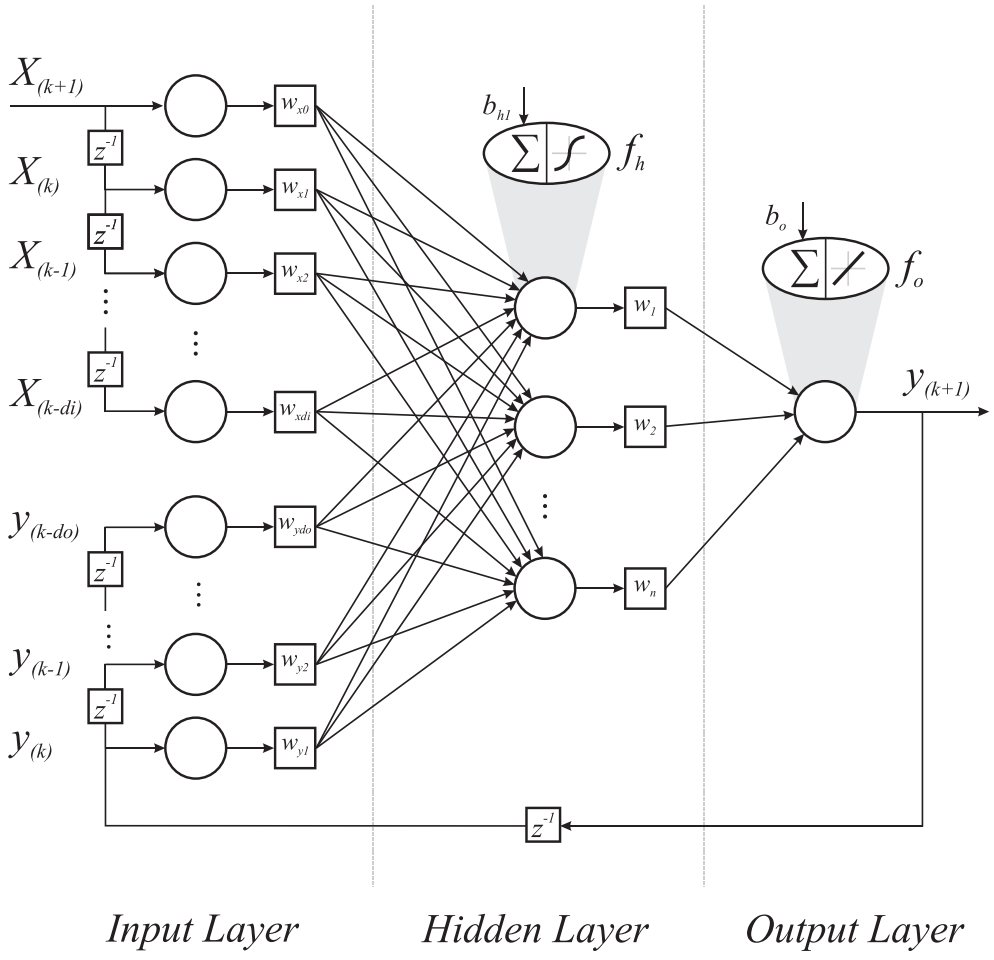

Fig. 6. Architecture of NARX neural networks.

Table 2
Tuned hyperparameters for MLP and NARX models.

Hyperparameter	Model	
	MLP	NARX
No. Hidden Layers	2	2
No. Neurons (1st Hidden Layers)	40	50
No. Neurons (2ed Hidden Layers)	10	25
Activation Function (1st Hidden Layers)	Tansig	Tansig
Activation Function (2ed Hidden Layers)	Tansig	Tansig
Activation Function (Output Layer)	Purelin	Purelin
Epochs	60	50
Training Algorithm	Bayesian regularization	Bayesian regularization
Delays	–	10

have a significant impact on the performance of deep learning model. It is important to choose test set from the same distribution and it must be taken randomly from all the data [64]. In this study, approximately 74% and 26% of the dataset were randomly divided for the training and testing subset, respectively. The random selection is to ensure that the train and test sets are representative of the original dataset.

In this work, Tansig is used as an activation function in the hidden layers, because it has had good performance in recent articles in this field [37]. However, utilization of novel activation functions also provides good performance in modeling [65].

4.3. Flow regimes

In this study, flow regimes have been investigated using the classic flow map of Mandhane et al. [24]. The flow pattern map is obtained experimentally for two-phase flow in the horizontal tube and the conditions of its use are listed in Table 3. By calculating the superficial velocities of oil and gas and matching them with the flow map, flow regimes are obtained for each sample (Fig. 7). For most of the test time, the flow regime is annular or close to the boundary between the annular flow and the slug flow (4100 points). This indicates that a large part of the data recorded is in the transition phase between the slug and annular flow regimes. Also in a few points, the flow regimes are slug (6 points), stratified (5 points), and wavy (1 point).

5. Results and discussion

Various statistical measures, such as coefficient of determination (R^2), absolute average percentage deviation (AAPD), and root mean squared error (RMSE), have been used for statistical analysis of the results [36,37,41]. The coefficient of determination R^2 indicates the ratio

Table 3
Range of parameter values for two-phase flow map.

μL (Pa.s)	μG (Pa.s)	σ (N/m)	D (mm)	ρL (kg/m^3)	ρG (kg/m^3)
0.0003–0.09	10^{-5} – 2.2×10^{-5}	0.024–0.1	12.7–165.1	705–1009	0.8–51

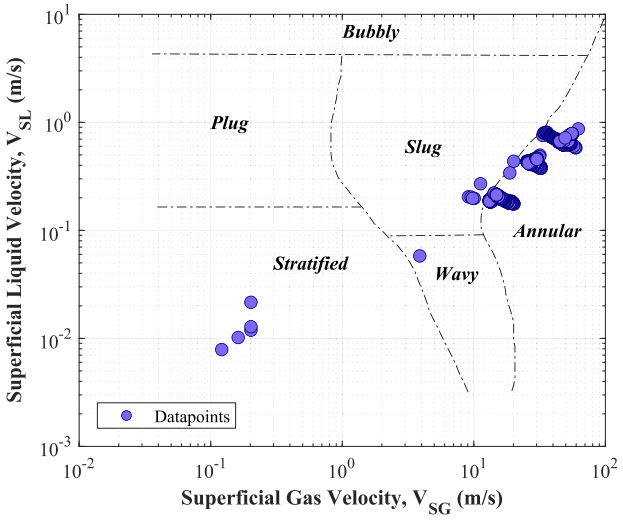

Fig. 7. Flow regimes distribution.

of variance of dependent variables, which can be predicted from independent variables and provides information about the quality of prediction of target values by the model. AAPD is the absolute mean relative deviation from the center point. The root mean squared error is widely used to measure the amount of error between measured and predicted data. Mathematical expressions of mentioned statistical measures are given in Equations (8) to (11), respectively. The closer the value of R^2 is to unity, the better the performance of the model is. On the other hand, a closer value of AAPD and RMSE to zero also indicates better performance of the predictive model.

$$R^2 = 1 - \frac{\sum_{i=1}^{N}\left(y_{\mathrm{Pred}}(i) - y_{\mathrm{Exp}}(i)\right)^2}{\sum_{i=1}^{N}\left(y_{\mathrm{Pred}}(i) - \bar{y}_{\mathrm{Exp}}\right)^2} \tag{8}$$

$$\%\ APD = \frac{100}{N}\sum_{i=1}^{N}\frac{\left(y_{\mathrm{Pred}}(i) - y_{\mathrm{Exp}}(i)\right)}{y_{\mathrm{Exp}}(i)} \tag{9}$$

$$\%\ AAPD = \frac{100}{N}\sum_{i=1}^{N}\left|\frac{y_{\mathrm{Pred}}(i) - y_{\mathrm{Exp}}(i)}{y_{\mathrm{Exp}}(i)}\right| \tag{10}$$

$$RMSE = \left(\frac{\sum_{i=1}^{N}\left(y_{\mathrm{Pred}}(i) - y_{Exp}(i)\right)^2}{N}\right)^{0.5} \tag{11}$$

The above statistical indicators are the most popular measures used to calculate and compare the accuracy of machine learning regression problems. RMSE is considered the most efficient statistical indicator utilized to measure the accuracy of regression problems. Mean square error (MSE) is used as loss function for training models. This loss function is given as a high penalty for wrong predictions. Other metrics can be used for regression problems, but R^2, RMSE, AAPD metrics are common in this field [36,37,41].

Tables 4-6 evaluate the performance accuracy of MLP and NARX models for training set, test set, and the overall dataset, respectively. Having a closer look at Table 4 reveals that the prediction accuracy of the NARX model was higher than the MLP model for the training and test sets. For oil flow rate prediction in the MLP model, RMSE = 7.18 m^3/day; AAPD = 1.02%; and R^2 = 0.9973. However, the oil flow rate prediction values in the NARX model are RMSE = 3.09 m^3/day; AAPD = 0.68%; and R^2 = 0.9995 (for the overall dataset).

For gas flow rate prediction in the MLP model, RMSE = 532.94 m^3/day; AAPD = 1.44%; and R^2 = 0.9973, while the same values in the NARX model are RMSE = 307.61 m^3/day; AAPD = 1.06%; and R^2 = 0.9991 (for the overall dataset).

In the MLP model, the RMSE of oil flow rate for test data was 10.10 m^3/day. However, gas flow rate prediction in the NARX model is 3.55 m^3/day. Also, in the MLP model, the RMSE of gas flow rate for test data is equal to 655.45 m^3/day, while the RMSE of the NARX model is equal to 318.62 m^3/day. The accuracy of model prediction for test data is important in measuring predictive ability for unseen or new data.

Fig. 8 shows the measured versus predicted oil and gas flow rates for the overall dataset. This diagram shows how the predicted value deviated from the actual value. If all the data is on the line with slope one, it indicates that the predicted values are equal to the actual measured values which is the ideal condition. In Fig. 8, the coefficient of determination is written on each diagram, which shows that the accuracy of the NARX model was higher in both oil and gas flow rate prediction compared to MLP model.

Fig. 9 and Fig. 10 show a comparison of the predicted oil and gas flow rates between the MLP and NARX models for training data and test data, respectively. The MLP model has made mistakes in predicting some points (e.g. 669th minute in the training set and 1034th minute in the testing set). However, Fig. 9 and Fig. 10 show that the NARX model is shown to be more accurate with less deviations from true values compared to MLP model.

During the tuning of hyperparameters (the parameters whose value is used to control the learning process), it was observed that data splitting will have a great impact on the accuracy of the model. This also highlights the importance of using large datasets that are effective in improving model accuracy.

The results obtained from the artificial neural network show that the prediction is in good agreement with the experimental data in different flow regimes. This subject is more important in high gas volume fractions and annular flow regimes because the uncertainties in measuring with commercial equipment in such flow regimes are significant.

The results show that the flow rate predicted by the neural network can follow the trend of the experimental data set. As observed in the literature, the neural network has performed well in predicting the gas flow through the choke, while the empirical equations have provided a high error [41]. The results of the analysis show that for own dataset the correlation of oil [37,38] and gas [41] flow with temperature and pressure is higher than in the literature. In this work, two features (temperature and pressure) were used as inputs of networks, which are less compared to the literature [38,41,44]. Research on feature engineering and feature selection can be considered as the topic of future research in this field.

Table 4
Prediction accuracy statistics for oil and gas flow rates in the training subset (3040 available data records; ~74%). Number of decimal places does not indicate accuracy of data.

Model	Phase	APD	AAPD	MSE	RMSE	R^2
		%	%	$(m^3/day)^2$	(m^3/day)	–
MLP	Oil	0.0435	0.8615	33.72	5.81	0.9983
	Gas	0.0957	1.1282	232,630	482.32	0.9978
NARX	Oil	0.0907	0.6917	8.51	2.92	0.9996
	Gas	0.4190	1.1556	92,187	303.62	0.9991

Table 5
Prediction accuracy statistics for oil and gas flow rates in the testing subset (1072 available data records; ~26%). Number of decimal places does not indicate accuracy of data.

Model	Phase	APD	AAPD	MSE	RMSE	R^2
		%	%	$(m^3/day)^2$	(m^3/day)	–
MLP	Oil	0.6317	1.4815	102.08	10.10	0.9947
	Gas	1.2686	2.3085	429,620	655.45	0.9959
NARX	Oil	0.0893	0.6641	12.59	3.55	0.9994
	Gas	0.0897	0.7771	101,520	318.62	0.9990

Table 6
Prediction accuracy statistics for oil and gas flow rates in the total dataset (4112 available data records; ~100%). Number of decimal places does not indicate accuracy of data.

Model	Phase	APD	AAPD	MSE	RMSE	R^2
		%	%	$(m^3/day)^2$	(m^3/day)	–
MLP	Oil	0.1969	1.0233	51.55	7.18	0.9973
	Gas	0.4017	1.4361	284,020	532.94	0.9973
NARX	Oil	0.0903	0.6845	9.57	3.09	0.9995
	Gas	0.3332	1.0569	94,622	307.61	0.9991

6. Conclusion

In the present study, a dynamic neural network was proposed to measure the two-phase flow rate of oil and gas with variable flow regimes and the obtained results were compared with the static network. The dataset comprising 4112 measured experimental samples was used to train the nonlinear autoregressive network with exogenous inputs (NARX) and multilayer perceptron (MLP). In trained networks, temperature and pressure are set as inputs for predicting oil and gas flow rates with variable flow regimes covering annular and slug flow, the transition phase between those two regimes as well as regimes indicated as slug, stratified and wavy.

About 74% of the total data was split for network training and about 26% of the data was used for network testing. In the NARX model, AAPD of 0.68% was found for oil flow rate prediction while AAPD of 1.02% was found for the MLP model. For gas flow rate prediction, NARX model gives AAPD of 1.06% while MLP model gives AAPD of 1.43%. The modeling results show that the NARX network can predict oil and gas flow with variable flow regimes more accurately than the MLP model. The simplicity of the MLP neural network structure is the main advantage of this network, which is the motivation for its development. The present work can hence be seen as a proof-of-concept study that should

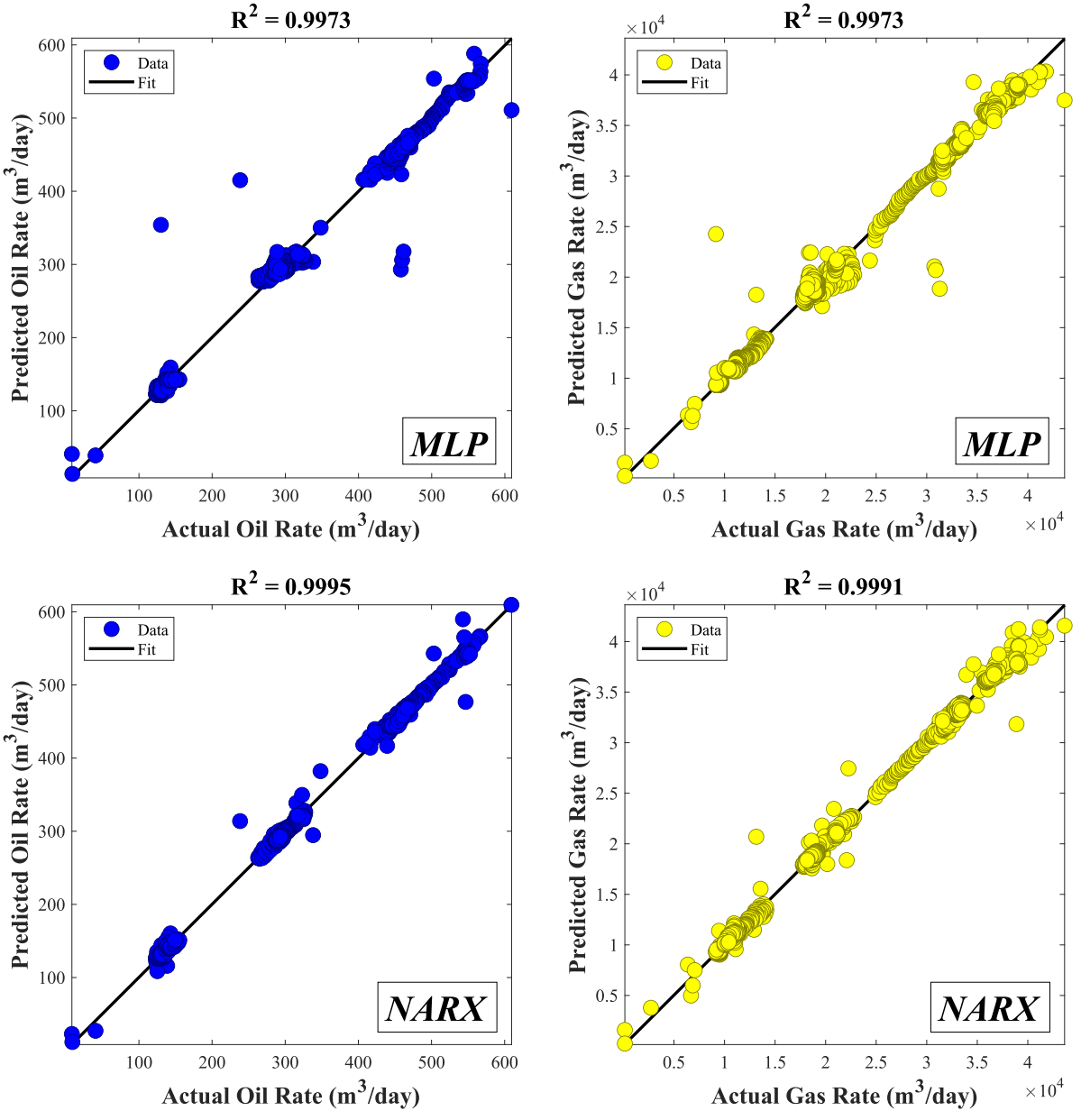

Fig. 8. Measured versus predicted oil and gas flow rates for overall dataset.

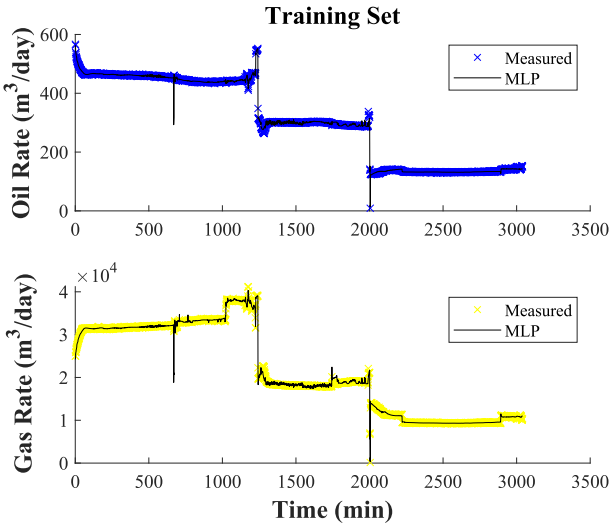

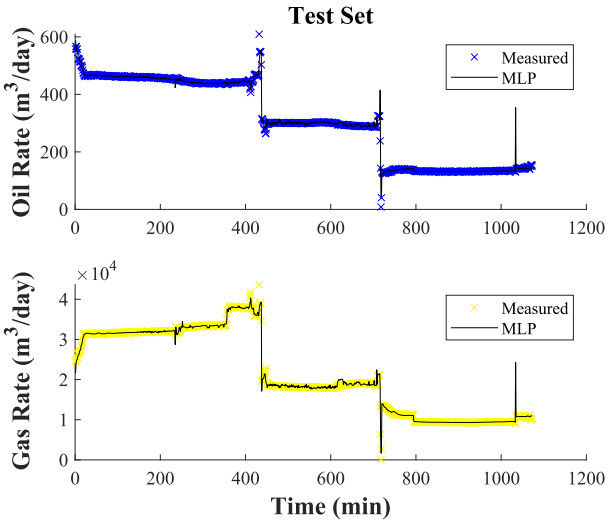

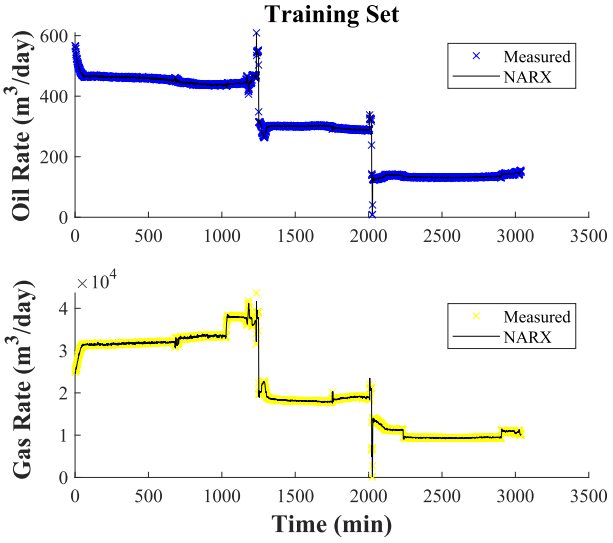

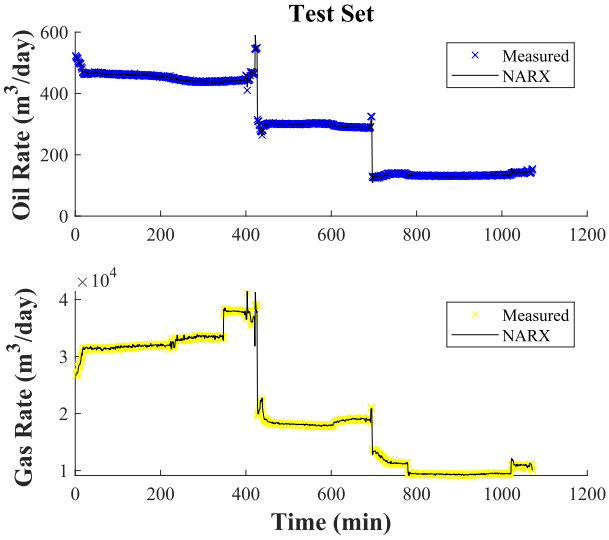

Fig. 9. Comparison of Measured and predicted oil and gas flow rates (training subset).

Fig. 10. Comparison of Measured and predicted oil and gas flow rates (testing subset).

motivate further applications of deep learning models to facilitate enhanced accuracy in flow meter readings when applied to flow regimes that are commonly qualitatively distinguished through visual means as is the case for gas–liquid mixtures.

The measurement of multiphase flows associated with high gas volume fractions, which are commonly associated with large uncertainties, can beneficially be improved by the use of machine learning methods. The combination of machine learning and multiphase flow meters needs more studying about robustness, proper methods, and input features.

CRediT authorship contribution statement

Mohammadreza Manami: Software, Methodology, Validation, Investigation, Formal analysis, Writing – original draft. **Sadegh Seddighi:** Conceptualization, Methodology, Project administration, Supervision, Writing – original draft. **Ramis Örlü:** Supervision, Writing – review & editing.

Declaration of Competing Interest

The authors declare that they have no known competing financial interests or personal relationships that could have appeared to influence the work reported in this paper.

Data availability

Data will be made available on request.

References

[1] D.H. Kim, T.I. Zohdi, R.P. Singh, Modeling, simulation and machine learning for rapid process control of multiphase flowing foods, Comput. Methods Appl. Mech. Eng. 371 (2020), 113286.

[2] F. Saberi-Movahed, M. Mohammadifard, A. Mehrpooya, M. Rezaei-Ravari, K. Berahmand, M. Rostami, S. Karami, M. Najafzadeh, D. Hajinezhad, M. Jamshidi, F. Abedi, M. Mohammadifard, E. Farbod, F. Safavi, M. Dorvash, N. Mottaghi-Dastjerdi, S. Vahedi, M. Eftekhari, F. Saberi-Movahed, H. Alinejad-Rokny, S. S. Band, I. Tavassoly, Decoding clinical biomarker space of COVID-19: Exploring matrix factorization-based feature selection methods, Comput. Biol. Med. 146 (2022), 105426.

[3] F. Saberi-Movahed, M. Najafzadeh, A. Mehrpooya, Receiving More Accurate Predictions for Longitudinal Dispersion Coefficients in Water Pipelines: Training Group Method of Data Handling Using Extreme Learning Machine Conceptions, Water Resour. Manag. 34 (2020) 529–561.

[4] H. Arastoopour, D. Gidaspow, R.W. Lyczkowski, Application of Multiphase Flow Simulation in Pharmaceutical Processes, in: H. Arastoopour, D. Gidaspow, R. W. Lyczkowski (Eds.), Transport Phenomena in Multiphase Systems, Springer International Publishing, Cham, 2022, pp. 299–316.

[5] M. Rahimi-Gorji, T.B. Gorji, M. Gorji-Bandpy, Details of regional particle deposition and airflow structures in a realistic model of human tracheobronchial airways: two-phase flow simulation, Comput. Biol. Med. 74 (2016) 1–17.

[6] M. Rahimi-Gorji, O. Pourmehran, M. Gorji-Bandpy, T.B. Gorji, CFD simulation of airflow behavior and particle transport and deposition in different breathing conditions through the realistic model of human airways, J. Mol. Liq. 209 (2015) 121–133.

[7] G. Falcone, G. Hewitt, C. Alimonti, Multiphase flow metering: principles and applications, Elsevier, 2009.

[8] M. Meribout, A. Azzi, N. Ghendour, N. Kharoua, L. Khezzar, E. AlHosani, Multiphase Flow Meters Targeting Oil & Gas Industries, Measurement 165 (2020), 108111.

[9] L.S. Hansen, S. Pedersen, P. Durdevic, Multi-Phase Flow Metering in Offshore Oil and Gas Transportation Pipelines: Trends and Perspectives, Sensors (Basel) 19 (2019) 2184.

[10] L. Xu, J. Xu, F. Dong, T. Zhang, On fluctuation of the dynamic differential pressure signal of Venturi meter for wet gas metering, Flow Meas. Instrum. 14 (2003) 211–217.

[11] S.R.V. Campos, J.L. Baliño, I. Slobodcicov, D.F. Filho, E.F. Paz, Orifice plate meter field performance: Formulation and validation in multiphase flow conditions, Exp. Therm. Fluid Sci. 58 (2014) 93–104.

[12] D.-H. He, B.-F. Bai, Two-phase mass flow coefficient of V-Cone throttle device, Exp. Therm Fluid Sci. 57 (2014) 77–85.

[13] D. He, B. Bai, Two-Phase Pressure Drop Prediction in Wet Gas Flow Through V-Cone Meter, 2014.

[14] R. Drury, A. Hunt, J. Brusey, Identification of horizontal slug flow structures for application in selective cross-correlation metering, Flow Meas. Instrum. 66 (2019) 141–149.

[15] High Performance Tester, Haimo America, Inc.

[16] J. Falcimaigne, S. Decarre, Multiphase production: pipeline transport, pumping and metering, Editions OPHRYS (2008).

[17] Vx Spectra, Surface multiphase flowmeter, Schlumberger.

[18] A. Karami, G.H. Roshani, A. Khazaei, E. Nazemi, M. Fallahi, Investigation of different sources in order to optimize the nuclear metering system of gas–oil–water annular flows, Neural Comput. & Applic. 32 (2020) 3619–3631.

[19] C. Marques Salgado, L.E.B. Brandão, R. Schirru, C.M.N.A. Pereira, A.X. da Silva, R. Ramos, Prediction of volume fractions in three-phase flows using nuclear technique and artificial neural network, Appl. Radiat. Isot. 67 (2009) 1812–1818.

[20] X. Shi, C. Tan, F. Dong, E.N.d. Santos, M.J.d. Silva, Conductance Sensors for Multiphase Flow Measurement: A Review, IEEE Sensors Journal, 21 (2021) 12913-12925.

[21] S. Corneliussen, J.-P. Couput, E. Dahl, E. Dykesteen, K.-E. Frøysa, E. Malde, H. Moestue, P.O. Moksnes, L. Scheers, H. Tunheim, Handbook of Multiphase Flow Metering, Norwegian Society for Oil and Gas Measurement (NFOGM), 2005.

[22] T. Bikmukhametov, J. Jäschke, First Principles and Machine Learning Virtual Flow Metering: A Literature Review, J. Pet. Sci. Eng. 184 (2020), 106487.

[23] Y. Yan, L. Wang, T. Wang, X. Wang, Y. Hu, Q. Duan, Application of soft computing techniques to multiphase flow measurement: A review, Flow Meas. Instrum. 60 (2018) 30–43.

[24] J.M. Mandhane, G.A. Gregory, K. Aziz, A flow pattern map for gas—liquid flow in horizontal pipes, Int. J. Multiph. Flow 1 (1974) 537–553.

[25] Y. Taitel, N. Lee, A. Dukler, Transient gas-liquid flow in horizontal pipes: Modeling the flow pattern transitions, AIChE J 24 (1978) 920–934.

[26] O. Baker, Design of Pipelines for the Simultaneous Flow of Oil and Gas, Fall Meeting of the Petroleum Branch of AIME, 1953.

[27] G.F. Hewitt, D.N. Roberts, Studies of two-phase flow patterns by simultaneous x-ray and flast photography, United Kingdom, 1969.

[28] E. Michaelides, C.T. Crowe, J.D. Schwarzkopf, Multiphase flow handbook, 2nd ed., CRC Press, Taylor & Francis Group, Boca Raton, 2017.

[29] G. Yadigaroglu, G.F. Hewitt, Introduction to multiphase flow: basic concepts, applications and modelling, Springer, 2017.

[30] L. Xu, W. Zhou, X. Li, S. Tang, Wet Gas Metering Using a Revised Venturi Meter and Soft-Computing Approximation Techniques, IEEE Trans. Instrum. Meas. 60 (2011) 947–956.

[31] A. Mirzaei-Paiaman, S. Salavati, The Application of Artificial Neural Networks for the Prediction of Oil Production Flow Rate, Energy Sources Part A 34 (2012) 1834–1843.

[32] I. Nejatian, M. Kanani, M. Arabloo, A. Bahadori, S. Zendehboudi, Prediction of natural gas flow through chokes using support vector machine algorithm, J. Nat. Gas Sci. Eng. 18 (2014) 155–163.

[33] H. Shaban, S. Tavoularis, Measurement of gas and liquid flow rates in two-phase pipe flows by the application of machine learning techniques to differential pressure signals, Int. J. Multiph. Flow 67 (2014) 106–117.

[34] N. Andrianov, A Machine Learning Approach for Virtual Flow Metering and Forecasting, IFAC-PapersOnLine 51 (2018) 191–196.

[35] T.A. Al-Qutami, R. Ibrahim, I. Ismail, M.A. Ishak, Virtual multiphase flow metering using diverse neural network ensemble and adaptive simulated annealing, Expert Syst. Appl. 93 (2018) 72–85.

[36] S. Rashid, A. Ghamartale, J. Abbasi, H. Darvish, A. Tatar, Prediction of Critical Multiphase Flow Through Chokes by Using A Rigorous Artificial Neural Network Method, Flow Meas. Instrum. 69 (2019), 101579.

[37] M. Farsi, H. Shojaei Barjouei, D.A. Wood, H. Ghorbani, N. Mohamadian, S. Davoodi, H. Reza Nasriani, M. Ahmadi Alvar, Prediction of oil flow rate through orifice flow meters: Optimized machine-learning techniques, Measurement 174 (2021), 108943.

[38] A.R. Behesht Abad, P.S. Tehrani, M. Naveshki, H. Ghorbani, N. Mohamadian, S. Davoodi, S.K.-y. Aghdam, J. Moghadasi, H. Saberi, Predicting oil flow rate through orifice plate with robust machine learning algorithms, Flow Measurement and Instrumentation, 81 (2021) 102047.

[39] A.F. Ibrahim, R. Al-Dhaif, S. Elkatatny, D. Al Shehri, Machine Learning Applications to Predict Surface Oil Rates for High Gas Oil Ratio Reservoirs, J. Energy Res. Technol. 144 (2021).

[40] A.A. Alakeely, R.N. Horne, Application of deep learning methods to estimate multiphase flow rate in producing wells using surface measurements, J. Pet. Sci. Eng. 205 (2021), 108936.

[41] A.R.B. Abad, H. Ghorbani, N. Mohamadian, S. Davoodi, M. Mehrad, S.K.-y. Aghdam, H.R. Nasriani, Robust hybrid machine learning algorithms for gas flow rates prediction through wellhead chokes in gas condensate fields, Fuel, 308 (2022) 121872.

[42] J. Mohamad-Saleh, B.S. Hoyle, Determination of multi-component flow process parameters based on electrical capacitance tomography data using artificial neural networks, Meas. Sci. Technol. 13 (2002) 1815–1821.

[43] M.M.F. Figueiredo, J.L. Goncalves, A.M.V. Nakashima, A.M.F. Fileti, R.D. M. Carvalho, The use of an ultrasonic technique and neural networks for identification of the flow pattern and measurement of the gas volume fraction in multiphase flows, Exp. Therm Fluid Sci. 70 (2016) 29–50.

[44] B. Bahrami, S. Mohsenpour, H.R. Shamshiri Noghabi, N. Hemmati, A. Tabzar, Estimation of flow rates of individual phases in an oil-gas-water multiphase flow system using neural network approach and pressure signal analysis, Flow Meas. Instrum. 66 (2019) 28–36.

[45] S. Chai, Z. Zhang, Z. Zhang, Carbon price prediction for China's ETS pilots using variational mode decomposition and optimized extreme learning machine, Ann. Oper. Res. (2021).

[46] Y. Raghuvamsi, K. Teeparthi, V. Kosana, A novel deep learning architecture for distribution system topology identification with missing PMU measurements, Results Eng. 15 (2022), 100543.

[47] G.H. Roshani, S.A.H. Feghhi, A. Mahmoudi-Aznaveh, E. Nazemi, A. Adineh-Vand, Precise volume fraction prediction in oil–water–gas multiphase flows by means of gamma-ray attenuation and artificial neural networks using one detector, Measurement 51 (2014) 34–41.

[48] H. Ghorbani, D.A. Wood, A. Choubineh, A. Tatar, P.G. Abarghoyi, M. Madani, N. Mohamadian, Prediction of oil flow rate through an orifice flow meter: Artificial intelligence alternatives compared, Petroleum 6 (2020) 404–414.

[49] F.M. White, Fluid mechanics, 6th ed., McGraw-Hill, New York, NY, 2009.

[50] Calculation of Flow through Nozzles and Orifices.

[51] ISO, ISO 5167-2: Measurement of fluid flow by means of pressure differential devices inserted in circular cross-section conduits running full - Part 2: Orifice plates, International Organization for Standardization, Switzerland, 2003.

[52] Aga, Aga 3.1: Orifice Metering of Natural Gas and Other Related Hydrocarbon Fluids, American Gas Association, 1990.

[53] M. Waskom, seaborn.pairplot.

[54] A.K. Palit, D. Popovic, Computational intelligence in time series forecasting: theory and engineering applications, Springer Science & Business Media, 2006.

[55] S. Haykin, Neural networks and learning machines, 3/E, Pearson Education India, 2010.

[56] S.M. Dassanayake, A. Mousa, G.J. Fowmes, S. Susilawati, K. Zamara, Forecasting the moisture dynamics of a landfill capping system comprising different geosynthetics: A NARX neural network approach, Geotext. Geomembr. (2022).

[57] A. Buevich, A. Sergeev, A. Shichkin, E. Baglaeva, A two-step combined algorithm based on NARX neural network and the subsequent prediction of the residues improves prediction accuracy of the greenhouse gases concentrations, Neural Comput. & Applic. 33 (2021) 1547–1557.

[58] W.-R. Zhang, T.-X. Liu, L.-M. Duan, S.-H. Zhou, L. Sun, Z.-M. Shi, S. Qu, M.-M. Bian, D.-G. Yu, V.P. Singh, Forecasting groundwater level of karst aquifer in a large mining area using partial mutual information and NARX hybrid model, Environ. Res. 213 (2022), 113747.

[59] H.T. Siegelmann, B.G. Horne, C.L. Giles, Computational capabilities of recurrent NARX neural networks, IEEE Transactions on Systems, Man, and Cybernetics, Part B (Cybernetics) 27 (1997) 208–215.

[60] L. Tsungnan, B.G. Horne, P. Tino, C.L. Giles, Learning long-term dependencies in NARX recurrent neural networks, IEEE Trans. Neural Netw. 7 (1996) 1329–1338.

[61] The-MathWorks-inc., Design Time Series NARX Feedback Neural Networks.

[62] M. Zhao, R. Zhang, C. Lin, H. Zhou, J. Shi, Stochastic Model Predictive Control for Dual-Motor Battery Electric Bus Based on Signed Markov Chain Monte Carlo Method, IEEE Access 8 (2020) 120785–120797.

[63] H. Wang, D. Hu, Y. Yang, M. Zhang, Multiphase flowrate measurement with time series sensing data and sequential model, 2021 IEEE International Instrumentation and Measurement Technology Conference (I2MTC), 2021, pp. 1-6.

[64] Cs230,, Splitting into train, dev and test sets, Stanford University, 2018.

[65] S.-L. Shen, N. Zhang, A. Zhou, Z.-Y. Yin, Enhancement of neural networks with an alternative activation function tanhLU, Expert Syst. Appl. 199 (2022), 117181.